Hypersonic Flow on Yawed Wedges with Leading-Edge Bluntness and Viscous Interaction

R. C. Boger* and G. F. Aiello†
Avco Systems Division, Wilmington, Mass.

A theoretical and experimental study of yawed two-dimensional bodies in a hypersonic stream, including the effects of leading-edge bluntness, viscous interaction, and small angle of attack, has been carried out. The theory due to Cheng et al., which was developed for the problem without yaw, is modified to treat the yawed case with the assumption that no gradients along the span exist in the flow over the body. The results of wind-tunnel tests, covering a wide range of Mach number and Reynolds number conditions at yaw angles of 60° and 70°, show that this major assumption is valid and verify the modified theory. These tests include the measurement of pressure, heat transfer, and total force on the body.

Nomenclature

C_H = surface heat-transfer coefficient $\dot{q}/\rho_\infty U_\infty \cos\Lambda(H_\infty - H_w)$
C = $\mu(T^*)/\mu(T_\infty)(T_\infty/T^*)$
d = length of the chord
D_N = drag of the blunt leading edge
h = specific enthalpy
H = total specific enthalpy $h + (u^2 + v^2)/2$
k = leading-edge (nose) drag coefficient $2D_N/\rho_\infty U_\infty{}^2 t$
K_ϵ = parameter related to the inviscid tip bluntness effect $(M\cos\Lambda)^3 \epsilon k t/x$
L = reference length
M = freestream Mach number
N = $M\cos\Lambda(C/Re_t)^{1/2}$, viscous interaction parameter
p = pressure
q = local surface heat-transfer rate
$Re_{L,x,t}$ = freestream Reynolds numbers based on $u_\infty \cos\Lambda$ and L, x or t
t = thickness of flat-face leading edge or diameter of cylindrical leading edge
T = temperature
T^* = reference temperature $T_0[1 + 3(T_w/T_0)]/6$
u,v,w = velocity components parallel to the x, y, and z axes, respectively
U_∞ = freestream velocity
x,y = rectangular coordinates, parallel and normal, to the freestream velocity (origin at model leading edge)
Y_b,Y_e / Y_s,Y_w = y ordinates of the inner edge of the entropy layer, the shock, and the body surface, respectively
z,ζ = variables related to Y_s and x, respectively [see Eqs. (14) and (15)]
α = angle of attack of flat plate, positive for compression angles
γ = specific heat ratio
Γ = parameter governing interactive effect of bluntness, displacement and incidence
δ,δ^* = boundary layer and displacement thickness
ϵ = limiting density ratio
θ = shock-wave angle, approximated by dY_s/dx
φ = viscosity
ρ = density
χ,χ_ϵ = parameters related to the boundary-layer displacement effect, $M_\infty{}^3\cos^3\Lambda(C/Re_x)^{1/2}$, $\epsilon[0.664 + 1.73(H_w/H_0)]\,M_\infty{}^3\cos^3\Lambda(C/Re_x)^{1/2}$
Λ = yaw angle
τ = $0.664 + 1.73\,T_w/T_0$

Subscripts

b,e = inner and outer edges of entropy layer
L = based on reference length
s = downstream side of shock wave
t = based on the nose thickness
w = at the body or wall
$0,\infty$ = isentropic stagnation and freestream conditions

Presented as Paper 70-783 at the AIAA 3rd Fluid and Plasma Dynamics Conference, Los Angeles, Calif., June 29–July 1, 1970; submitted July 16, 1970; revision received February 23, 1971. This research was supported by the Space and Missile Systems Organization, Air Force Systems Command. The authors gratefully acknowledge the generous assistance of several of their coworkers at Avco Systems Division.

* Senior Staff Scientist, Applied Science Directorate. Associate Member AIAA.
† Senior Staff Scientist, Applied Science Directorate.

Introduction

THE problem of hypersonic flow past a two-dimensional body with the combined effects of leading-edge bluntness and viscous interaction was considered by Cheng et al.[1] They showed that a theory based upon blast-wave pressure combined with the boundary-layer displacement effect was in good agreement with their experimental results over a wide range of test conditions. Recently Kemp[2] suggested a modification to the theory for $\gamma > 1$. He has shown this modified theory agrees with the experimental data he obtained at Mach number 42 in helium.

The theory is extended in this paper to treat yawed bodies as shown in Fig. 1. Because of the yaw, the relative importance of the bluntness and viscous interaction effects changes. Their contributions to drag, for example, are such that the leading-edge pressure drag is diminished by yaw so that the viscous drag can dominate. The major new assumption required to modify the theory is that no gradients along the span exist in the flow. A series solution to the governing equation in Cheng's theory is developed to show the important parameters and to expedite the theoretical predictions of the test results. The first-order corrections[2] for $\gamma > 1$ are also included.

Wind-tunnel tests were conducted at the von Kármán Gas Dynamics Facility, AEDC with the slab and wedge configurations shown in Fig. 2 yawed at 60° and 70° to the flow, to check the assumption of no gradients along the span and to obtain distributions along the chord of surface pressure and heat transfer. Force measurements were also made in a portion of the tests. The results are compared with theory and the limitations suggested by this comparison are discussed.

Theory

Assumptions

This paper will parallel the development of Ref. 1 when the leading-edge is yawed at some angle Λ to the flow. The bluntness gives rise to an increased surface pressure, persist-

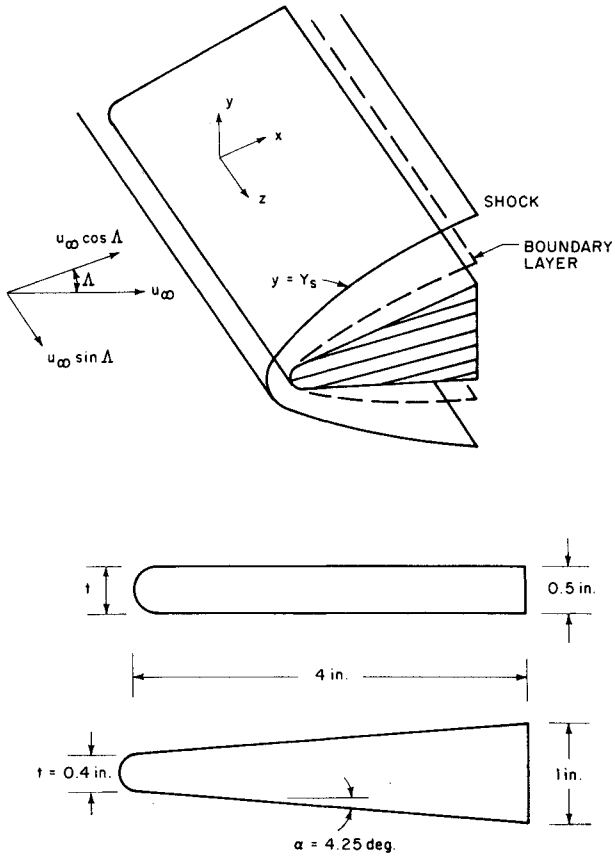

Fig. 1 Yawed body geometry.

ing downstream of the nose. This effect is treated by considering the entropy layer created at the nose, and the overpressure is found to decay in a manner analogous to a blast wave. The boundary layer displaces the external flow and gives rise to an additional increase in pressure. For a slightly blunted wedge both the nose bluntness and viscous interaction effects are gradually lost far downstream on the wedge surface.

The analysis is limited by four requirements: a) the disturbance velocity, $\Delta u/u_\infty = (u/u_\infty - 1)$ as well as the square of the flow angle in the inviscid flowfield, must be negligibly small compared to unity; b) the bow shock must be sufficiently strong; c) the specific heat ratio γ must be sufficiently close to unity; and d) there is no variation in the flow along the span. Requirement (a) excludes the nose region. The consistency of requirements (a–c) and the approximations involved are discussed by Cheng.[1]

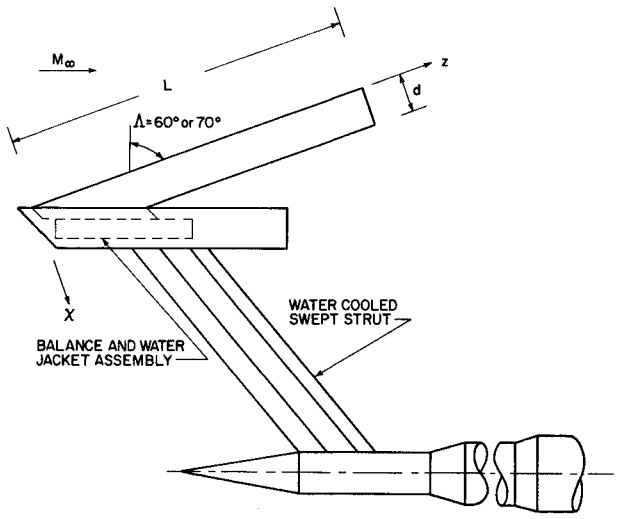

Fig. 2 Installation in tunnel C.

Local Boundary Layer Similarity

When the usual yawed wing assumption of no variation along the span ($\partial/\partial z = 0$) is made, the equations for the boundary layer become

$$\partial(\rho u)/\partial x + \partial(\rho v)/\partial y = 0 \quad (1)$$

$$\rho u\, \partial u/\partial x + \rho v\, \partial u/\partial y = -\partial p/\partial x + (\partial/\partial y)(\mu\, \partial u/\partial y) \quad (2)$$

$$\rho u\, \partial w/\partial x + \rho v\, \partial w/\partial y = (\partial/\partial z)(\mu\, \partial w/\partial y) \quad (3)$$

$$\partial p/\partial y = 0 \quad (4)$$

$$\rho u\, \partial H/\partial x + \rho v\, \partial H/\partial y = (\partial/\partial y)[(\mu/Pr)\partial H/\partial y] - (\partial/\partial y)\{\mu(1/Pr - 1)(\partial/\partial y)[(u^2 + w^2)/2]\} \quad (5)$$

We shall assume that $Pr = 1$. These equations may be compared with those given by Reshotko and Beckwith[3] or Dewey.[4] The variables are transformed from x, z to ξ, η by defining

$$\xi = \int_0^x \frac{C p d\chi}{p_\infty L}, \quad \eta = \left(\frac{Re_L}{\xi}\right)^{1/2} \int_0^y \frac{\rho dy}{\rho_\infty L} \quad (6)$$

The reference temperature

$$T^* = T_0[1 + 3T_w/T_0]/6$$

is used in obtaining

$$C = \mu(T^*)T_\infty/[\mu(T_\infty)T^*]$$

The nondimensional variables are given by

$$u/u_\infty \cos\Lambda = f' = \partial f/\partial\eta$$

$$w/u_\infty \sin\Lambda = g, \quad (H - H_w)/(H_\infty - H_w) = \Theta$$

and they satisfy the equations

$$2f_{\eta\eta\eta} + f f_{\eta\eta} - 2\xi[f_\eta f_{\xi\eta} - f_\xi f_{\eta\eta}] = \epsilon\left[\left(2\frac{dp}{dx}\int_0^x p dx\right)\Big/p^2\right]\left[\frac{T_w}{T_0} + \left(1 - \frac{T_w}{T_0}\right)\Theta - f^2\right]$$

$$2g_{\eta\eta} + f g_\eta - 2\xi[f_\eta g_\xi - f_\xi g_\eta] = 0$$

$$2\Theta_{\eta\eta} + f\Theta_\eta - 2\xi[f_\eta\Theta_\xi - f_\xi\Theta_\eta + f_\eta\Theta(d/d\xi)\ln(1 - T_w/T_0)] = 0$$

The boundary conditions to be fulfilled are

$$f = f_\eta = g = \Theta = 0 \quad \text{at} \quad \eta = 0$$

$$f_\eta = g = \Theta = 1 \quad \text{at} \quad \eta = \infty$$

The leading term in the solution for small $\epsilon = (\gamma - 1)/(\gamma + 1)$ will be independent of ξ, and similarly the effect of pressure gradient does not enter into the zero-order solution. Hence the equations become

$$2f''' + ff'' = 0, \quad 2g'' + fg' = 0, \quad 2\Theta'' + f\Theta' = 0$$

The solutions of the second and third equations are expressible as $g = f'$, $\Theta = f'$, so the boundary-layer problem is reduced to the Blasius equation.

The surface heat-transfer coefficient

$$C_H = \dot{q}/\rho_\infty u_\infty \cos\Lambda(H_\infty - H_w) \quad (7)$$

is determined explicitly from the surface pressure distribution as

$$C_H = 0.332\left(\frac{C}{Re_L}\right)^{1/2}\left(\int_0^x \frac{p dx}{p_\infty L}\right)^{-1/2}\frac{p}{p_\infty}$$

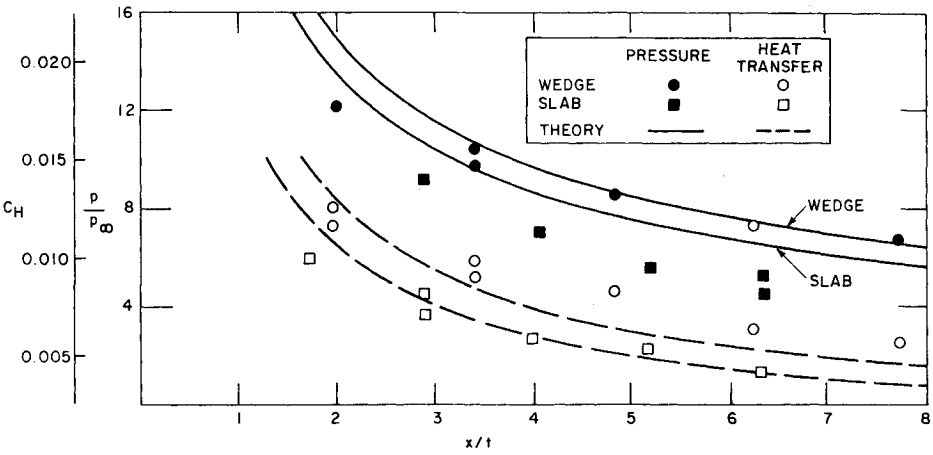

Fig. 3 Pressure and heat transfer, $M = 18.7$, $Re = 0.069 \times 10^6$, $\Lambda = 60°$.

The skin friction coefficient $C_f = 2\tau/\rho_\infty U_\infty^2$ is found to act in the stream direction and is related to heat transfer by

$$C_f = 2C_H \cos\Lambda \tag{8}$$

Finally, the boundary-layer displacement thickness is given by

$$\frac{\delta^*}{L} = \epsilon\tau\chi_L \left(\int_0^x \frac{p\,dx}{p_\infty L}\right)^{1/2} \frac{p_\infty}{pM\cos\Lambda}$$

where

$$\chi_L = (M\cos\Lambda)^3(C/Re_L)^{1/2} \tag{9}$$

and $\tau = 0.664 + 1.73\ T_w/T_0$.

Tip Bluntness Effect and Detached Shock Layer

The analysis of the detached shock layer in the x direction is identical to Cheng's. The blastwave analogy states that the pressure on the surface is related to the energy deposited in the flow at the blunt nose. The essential features of this analysis will be summarized here.

The shock layer is assumed to lie at the outer edge of the entropy layer at $y = Y_e$. The pressure there is given by the Newton-Busemann formula, $p_e = \rho_\infty(U_\infty \cos\Lambda)^2(Y_eY_e')'$, where the prime now denotes differentiation with respect to x.

The entropy layer has essentially constant pressure from its outer edge, Y_e, to the body Y_b. This allows a simple expression to be derived for the flow in it. In particular its outer edge is defined by

$$(Y_e - Y_b)(Y_eY_e')' = \epsilon kt/2 \tag{10}$$

where $\epsilon = (\gamma - 1/\gamma + 1)$, k is the nose drag coefficient (unyawed) and t is the nose thickness.

Viscous Interaction

To account for the displacement of the outer flow by the thickening boundary layer along the body, Cheng introduces a simple and direct procedure. The body location Y_b is changed to an apparent body location $Y_b + \delta^*$, so that Eq. (10) becomes

$$(Y_e - Y_b - \delta^*)(Y_eY_e')' = \epsilon kt/2 \tag{11}$$

and

$$\delta^* = \epsilon\tau\chi_L(LY_eY_e')^{1/2}/(M\cos\Lambda)^2(Y_eY_e')'$$

It is convenient to introduce one variable which describes bluntness effects,

$$K_\epsilon = (M\cos\Lambda)^3\epsilon kt/x \tag{12}$$

and another for viscous effects,

$$\chi_\epsilon = \epsilon\tau(M\cos\Lambda)^3(C/Re_x)^{1/2} \tag{13}$$

These are used to form new independent and dependent variables, through

$$z = 8M\cos\Lambda(\chi_\epsilon/K_\epsilon)^2(Y_e/x) = 8\epsilon\tau^4N^4Y_e/k^3t \tag{14}$$

$$\zeta = 16[\chi_\epsilon K_\epsilon^{-2/3}]^6 = 16(x/t)\epsilon^2(\tau N)^6/k^4 \tag{15}$$

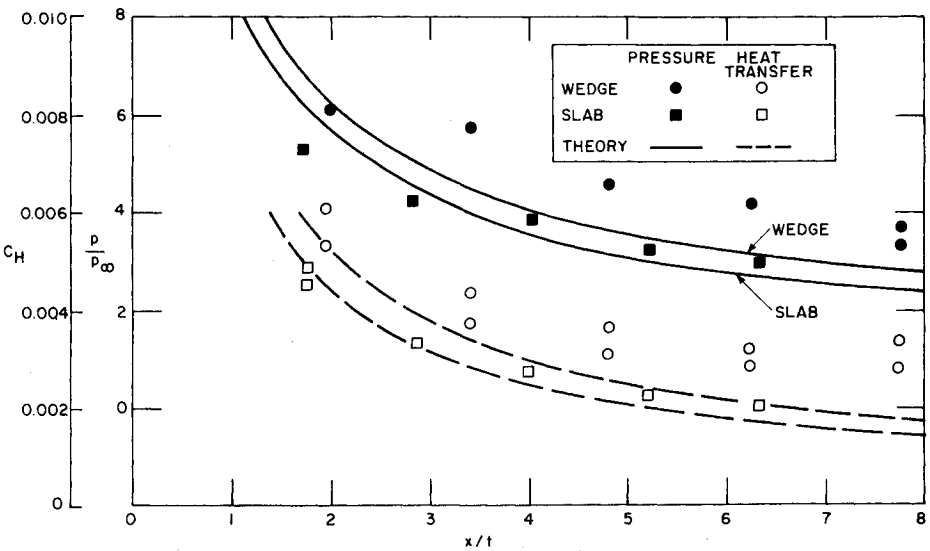

Fig. 4 Pressure and heat transfer, $M = 18.4$, $Re = 0.305 \times 10^6$, $\Lambda = 70°$.

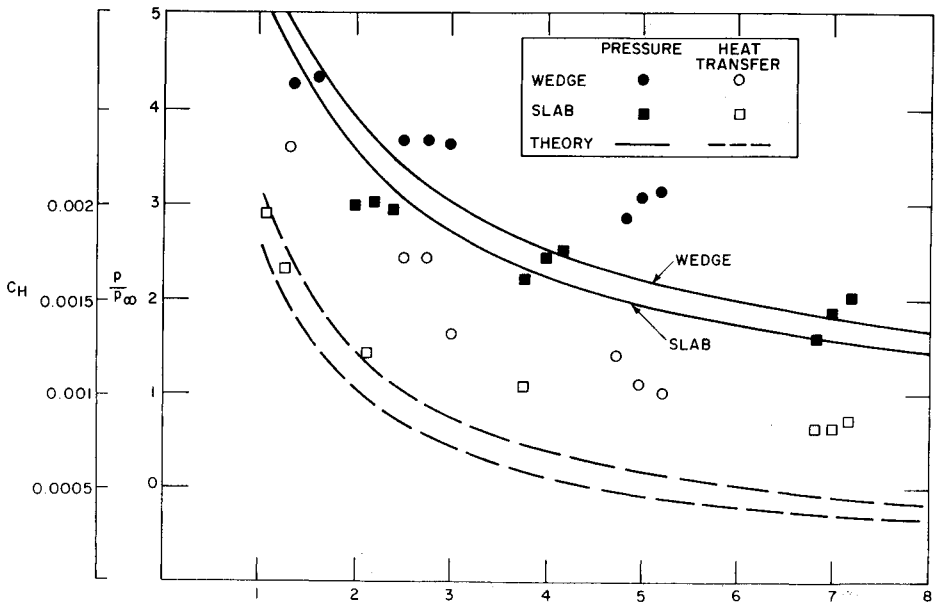

Fig. 5 Pressure and heat transfer, $M = 10.2$, $Re = 2.4 \times 10^6$, $\Lambda = 60°$.

where $N = M \cos\Lambda\,(C/Re_t)^{1/2}$. Equation (11) now becomes

$$(z - \Gamma\zeta)(zz')' - (zz')^{1/2} = 1 \tag{16}$$

Here Γ is a parameter independent of x given by

$$\Gamma = k\alpha/2\epsilon c\tau^2N^2 \tag{17}$$

The physical quantities of interest are now expressible as

$$p_w/p_\infty = 4\gamma\epsilon^2(M\ \cos\mathrm{A})^2(\tau N)^4(zz')'/k^2$$

and

$$C_H = 2.656\gamma^{1/2}\epsilon^2\tau^5N^6(zz')'/k^3(zz')^{1/2}$$

The total drag in the stream direction is composed of the nose drag, the integrated skin friction on the sidewalls, and the component of sidewall pressure in the stream direction. The drag coefficient, $2D/\rho_\infty u_\infty^2 t$, is found to be

$$C_D = k\ \cos\mathrm{A}[\cos^2\mathrm{A} + 1.328(\gamma zz')^{1/2}/\tau + \alpha kRe_t zz'/CM^2\tau^2] \tag{18}$$

where the three terms correspond, respectively, to the three sources of drag mentioned previously.

Corrections for γ Not Equal to One

Kemp[2] has proposed a modification to Cheng's theory for the first order effects of γ not equal to one. The modification is accomplished by factors composed of γ and $A = (\gamma + 1)/2$. The quantities of interest become

$$z = (A^4/\gamma^2)8\epsilon\tau^4N^4Y_e/k^3t \tag{14a}$$

$$\zeta = (A^7/\gamma^3)16(x/t)\epsilon^2(\tau N)^6/k^4 \tag{15a}$$

$$\Gamma = (\gamma/A^2)k\alpha/2\epsilon\tau^2N^2 \tag{17a}$$

$$p_w/p_\infty = (A^5/\gamma^2)4\gamma\epsilon^2(M\ \cos\mathrm{A})^2\tau^4N^4(zz')'/k^2$$

$$C_H = (A^6/\gamma^{5/2})2.656\gamma^{1/2}\epsilon^2\tau^5N^6(zz')'/k^3(zz')^{1/2}$$

$$C_D = k\ \cos\mathrm{A}[\cos^2\mathrm{A} + 1.328(\gamma^{1/2}/A)(\gamma zz')^{1/2}/\tau + (\gamma/A^2)\alpha kRe_t zz'/CM^2\tau^2] \tag{18a}$$

The governing Eq. (16) is unchanged.

Theoretical Results

The solution to Eq. (16) is expressed by the series

$$z = 1.65096\zeta^{2/3}[1 + 0.30812\zeta^{1/6} + (0.10095\Gamma - 0.01508)\zeta^{1/3} + 0(\zeta^{7/6})]$$

The pressure is found to be

$$p_b/p_\infty = A^{1/3}0.38157\gamma\epsilon^{2/3}k^{2/3}(M\ \cos\mathrm{A})^2(t/x)^{2/3} \times [1 + 1.0399\zeta^{1/6} + (0.50475\Gamma + 0.16194)\zeta^{1/3}]$$

and the heat transfer is

$$C_H = A^{1/6}\,0.11840\gamma^{1/2}(\epsilon k)^{1/3}N(t/x)^{5/6} \cdot [1 + 0.6933\zeta^{1/6} + (0.37856\Gamma + 0.23563)\zeta^{1/3}]$$

To compare this with the wind-tunnel data, we have (including Kemp's correction) for $\gamma = 1.4$ and $\epsilon = 1/6$

$$\zeta^{1/6} = 0.7539\tau N(x/t)^{1/6} \tag{19}$$

The pressure, heat transfer, and drag can then be expressed as

$$P_b/P_\infty = 0.2082(M\ \cos\mathrm{A})^2(t/x)^{2/3}[1 + 0.7840\tau N(x/t)^{1/6} + (0.2889\Gamma + 0.09204)\tau^2N^2(x/t)^{1/3}] \tag{20}$$

$$C_H = 0.08746N(t/x)^{5/6}[1 + 0.5227\tau N(x/t)^{1/6} + (0.2152\Gamma + 0.1399)\tau^2N^2(x/t)^{1/3}] \tag{21}$$

$$C_D = k\ \cos^3\mathrm{A} + 2.099\ \cos\Lambda N(x/t)^{1/6}[1 + 0.2613\tau N(x/t)^{1/6} + (0.07173\Gamma + 0.04463)\tau^2N^2(x/t)^{1/3} + 1.7846\alpha\ \cos^3\Lambda(x/t)^{1/3}[1 + 0.5227\tau N(x/t)^{1/6} + (0.1434\Gamma + 0.04602)\tau^2N^2(x/t)^{1/3}] \tag{22}$$

Note that

$$\Gamma = 3.888\ \alpha/\tau^2N^2$$

Table 1 Tunnel C instrument locations[a]

Span location (z/L) of pressure taps	Chord location (x/d) of pressure taps
0.55	0, 0.135, 0.275, 0.495, 0.875
0.75	0, 0.160, 0.300, 0.520, 0.900
0.95	0, 0.185, 0.315, 0.545, 0.925

[a] Heat-transfer gages are located 0.1 in. beyond pressure taps (z axis) and 0.1 in. closer to the leading edge (x axis).

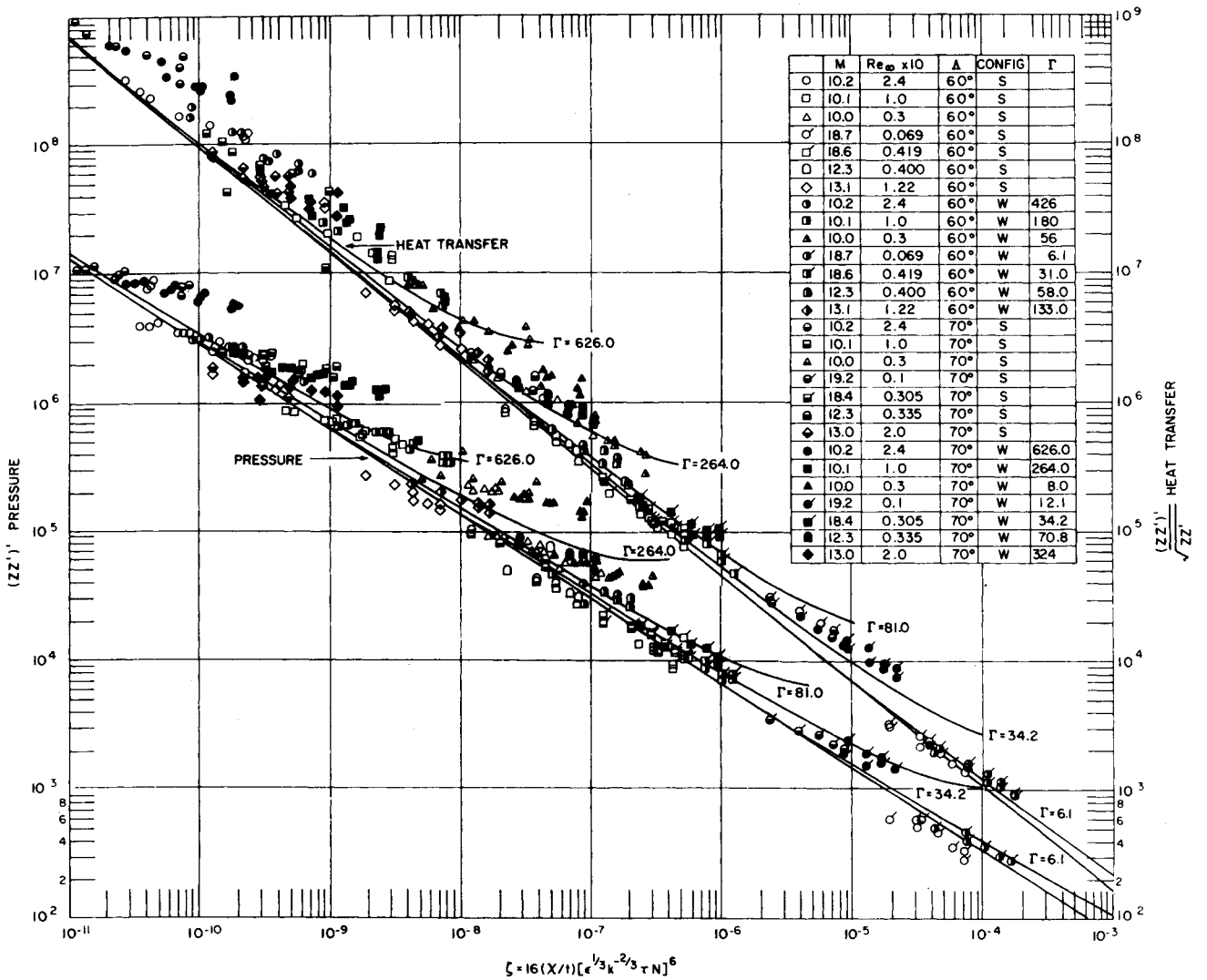

Fig. 6 Correlation of pressure and heat-transfer data.

Test Description

The tests were carried out in AEDC's Tunnels C and F. Tunnel C is a Mach 10, continuous flow, 50-in.-test-section wind tunnel with a Reynolds number capability of 0.3×10^6 to 2.4×10^6/ft. A model injection system allows the models to be injected and retracted from the flow without interrupting the tunnel's operation. Tunnel F is a hypervelocity arc-driven facility with useful run duration of about 150 msec. It has a 4.5-ft-diam section operating at Mach 12 to 13 and $Re = 0.8$ to 1.7×10^6/ft, and a 9.0-ft-diam section operating at Mach 19 to 20 with $Re = 0.04$ to 0.8×10^6/ft.

The heat flux was measured using low-level calorimeters positioned chordwise along the element at a number of span locations. Surface pressures were obtained at similar stations (see Tables 1 and 2). In Tunnel C, the elements were individually tested on a flat plate mounting shown in Fig. 2; in Tunnel F the elements were tested in pairs mounted on a slender cone-cylinder. Two pairs of models were used in the testing. The first pair had semicircular leading edges and slab afterbodies with side-walls parallel to the freestream ($\alpha = 0$). Their yaw angles were 60° and 70°. The second pair differed from the first only in the angle of the sidewalls as shown in Fig. 1. These were inclined at $\alpha = 4.25°$. Here-

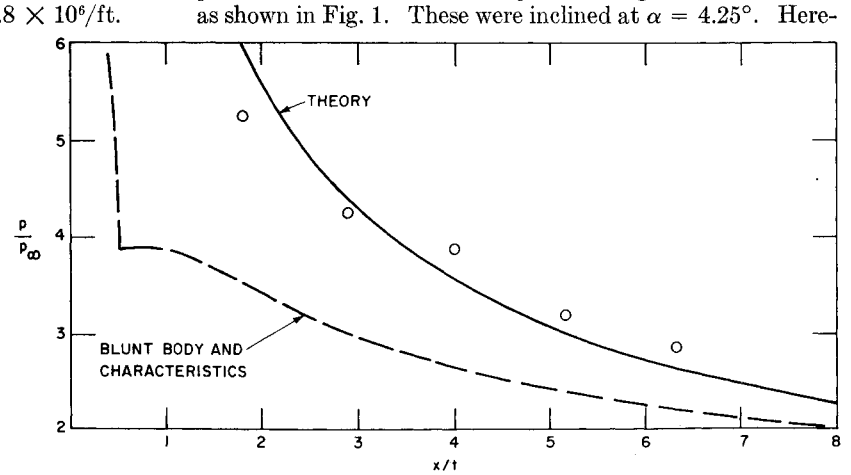

Fig. 7 Comparison of exact inviscid calculation with present results for slab at $\Lambda = 70°$, $M = 18.4$ $M\cos\Lambda = 6.3$, $Re_\infty = 0.305 \times 10^6$.

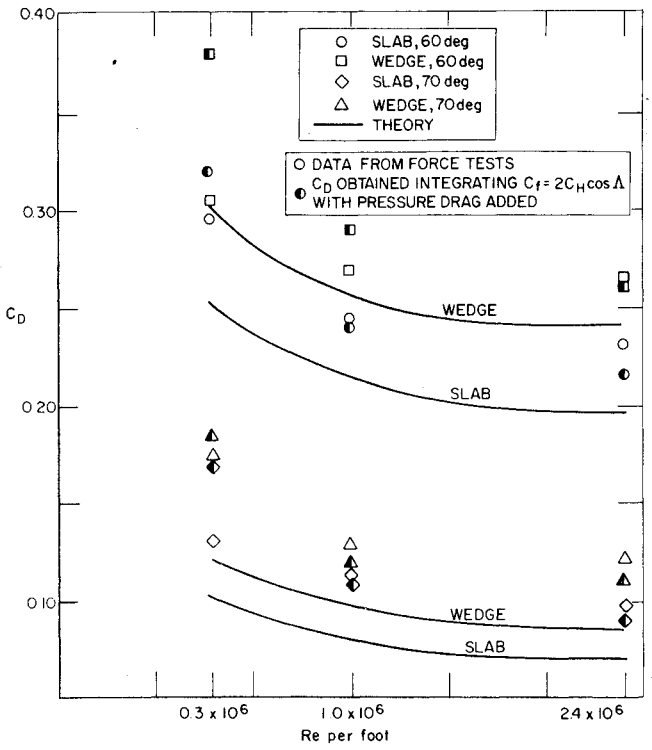

Fig. 8 Measured drag coefficient.

after, these models will be called the slab and wedge, respectively. Note that in Tunnel C the same instrument locations apply to both the 60° and 70° yaw angles, whereas in Tunnel F the locations differ for the two yaw angles.

Force and moment measurements were made in Tunnel C only, utilizing the same support shown in Fig. 2 for the pressure and heat transfer tests. The instrumented slab or wedge model was removed and replaced by a similar force configuration. The forces and moments acting on this model were measured using a 6-component balance internally mounted within the supporting flat plate. The same two yaw angles, 60° and 70° were tested with the flat plate at zero angle of attack.

Test Results

The tests covered M_∞ from 10 to 19.2, Re_t from 1140 to 50,000, and N from 0.0167 to 0.218. The upper end of this range approaches the rarefied flow regime.

Table 2 Tunnel F instrument locations[a]

Span locations (z/L) of heat-transfer gages
60° Sweep: 0.583, 0.903
70° Sweep: 0.558, 0.933
Chord locations (x/d) of heat-transfer gages
Slab: 0.215, 0.359, 0.503, 0.646, 0.790
Wedge: 0.1975, 0.340, 0.483, 0.625, 0.774

[a] Pressure taps are located at same x/d values as heat-transfer gauges but 0.375 in. further inboard (z axis)

The test results showed that the assumption the gradients across the span are vanishingly small is reasonable, and the only span gradients that did occur formed no consistent pattern. Figures 3–5 show examples of the experimental pressure and heat-transfer data and corresponding theoretical predictions. In general, the theory was in reasonable agreement with the experimental results.

All of the data are compared with the theory in Fig. 6 in a manner similar to Cheng's.[1] The theoretical curve was generated by numerically integrating Eq. (16). The branches corresponding to different values of the wedge parameter are also shown. The viscous interaction increases with increasing ζ, and as mentioned earlier, the merged layer regime is approached for the largest values achieved in the tests. The over-all agreement is good, with the higher Mach number test data showing better agreement.

A major feature of the theory is that the pressure varies in a manner governed by blast-wave similarity. Therefore, the pressure is highest at the nose and decays towards the trailing edge, and the heat transfer has a similar behavior. However, the theory has a singularity at the leading edge, and it cannot be expected to predict experimental results in that vicinity. The question of just how close to the leading edge the blast-wave predictions are expected to apply has not been settled. Stewartson and Thompson[5] have recently pointed out the theoretical difficulties that exist. As a basis for comparing the theoretical predictions and the experimental data, a two-dimensional blunt-body and method-of-characteristics program[6] was used to obtain the pressure variation along the slab model. The normal component of the Mach number was input as the freestream Mach number into the program. One case is illustrated in Fig. 7 for 70° yaw with $M = 18.4$, $M\cos 70° = 6.3$, and $Re_\infty = 0.305 \times 10^6$. The present theory predicts substantially higher pressure near the leading edge than does the method-of-characteristics solution. However, the data are closer to the prediction obtained from the theory. This was also the case for the other comparisons which were made.

The physical behavior of the boundary layer in the vicinity of the juncture between the cylindrical leading edge and the

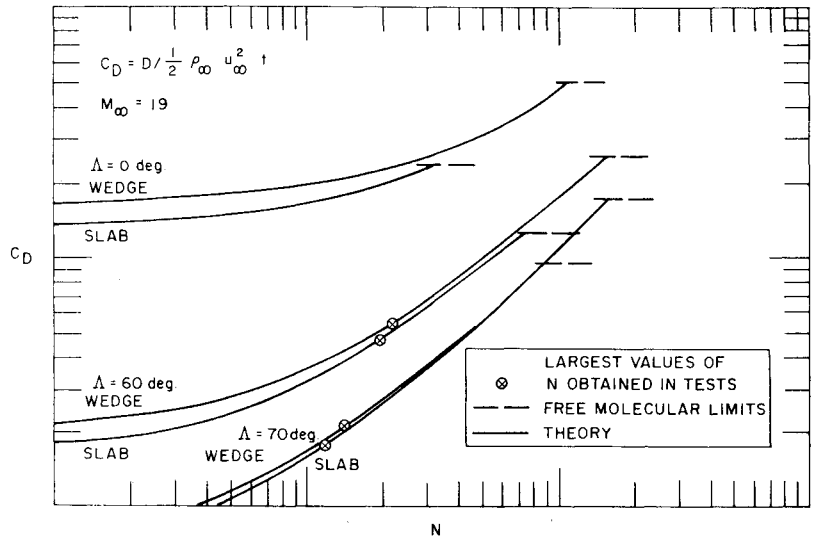

Fig. 9 Variation of C_D with N.

straight afterbody smooths the abrupt pressure decrease indicated by the characteristics solution. The present theory makes no pretense of treating this difficult problem, but it has been considered by Fannelop and Flugge-Lotz.[7] Although the theory developed here is not intended to apply right at the nose, it does account for the viscous interaction due to boundary-layer growth away from the leading edge.

The data obtained from the Mach 10 tests show a variation of pressure and heat transfer with Reynolds number that is not predicted by the present theory. The likely explanation for this discrepancy is that the value of $M\cos\Lambda$ is low enough to invalidate the theoretical assumptions. For 70° yaw it is only 3.4. The boundary-layer interactions that occur under these conditions are such that they overpower the weak pressure increment due to the blunt leading edge.

Drag Tests

Drag measurements were made in Tunnel C over the full Re range available. The drag is composed of viscous and inviscid portions with the viscous drag predominating for high Λ and large N. In the present tests the viscous drag accounted for 14–47% of the total drag according to the theory. However the pressure and heat transfer measurements in Tunnel C were generally higher than predicted. It is not surprising, therefore, that the measured values of C_D shown in Fig. 8 are higher than the theoretical values. Nevertheless, the variation of C_D with Reynolds number is in qualitative agreement with the theory.

As a check of consistency, the experimental heat transfer was curve-fitted and integrated, the skin friction was obtained using Reynolds analogy, and the pressure drag was added to obtain the total drag. The points obtained in this manner are shown in Fig. 8, and they generally agree with the measured drag. This technique is quite crude, of course, because the heat-transfer measurements allow only a rough curve fit to be made.

The increase in the viscous drag contribution and the approach to rarefied flow is indicated in Fig. 9, where the zero yaw case is included for comparison. Along the right hand side the free molecular limits are indicated, and each theoretical curve is terminated at that level. As Λ increases, the variation of C_D with N increases, indicating the greater relative contribution of viscous forces. The highest values of this parameter achieved in the Tunnel F tests are indicated, and they are well into the range where viscous forces dominate. In fact, rarefaction effects are to be expected here.

Conclusions

Tests have shown that the modified theory of Cheng et al., developed here yields useful data correlations for a blunt two-dimensional wedge (or slab) yawed with respect to a hypersonic stream. The major theoretical assumption of no span gradients in the flow appears to be acceptable over a wide range of the test conditions for yaw angles of 60° and 70°. This assumption should therefore be acceptable for similar flow conditions and smaller yaw angles. The theoretical results are in fair agreement with the experimental values of pressure, heat transfer, and drag. Some deviations occur at the lowest values of $M\cos\Lambda$, where the overpressure predicted by the blast wave analogy are small.

References

[1] Cheng, H. K., Gall, J. G., Golian, T. C., and Hertzberg, A., "Boundary-Layer Displacement and Leading-Edge Bluntness Effects in High-Temperature Hypersonic Flow," *Journal of the Aerospace Sciences*, Vol. 28, No. 5, May 1961, pp. 353–381.

[2] Kemp, J. H., Jr., "Hypersonic Viscous Interaction on Sharp and Blunt Inclined Plates," *AIAA Journal*, Vol. 7, No. 7, July 1969, pp. 1280–1289.

[3] Reshotko, E. and Beckwith, I. E., "Compressible Laminar Boundary Layer Over a Yawed Infinite Cylinder with Heat Transfer and Arbitrary Prandtl Number," Rept. 1379, 1958, NASA.

[4] Dewey, C. F., Jr., "Use of Local Similarity Concepts in Hypersonic Viscous Interaction Problems," *AIAA Journal*, Vol. 1, No. 1, Jan. 1963, pp. 20–32.

[5] Stewartson, K. and Thompson, B. W., "Eigenvalues for the Blast Wave," *The Physics of Fluids*, Vol. 13, No. 2, Feb. 1970, pp. 227–236.

[6] Gustafson, G., "User Instructions for Modified NASA Ames Blunt-Body and Method-of-Characteristics Program," K210-TR-67-140, Nov. 1967, Avco Systems Div., Wilmington, Mass.

[7] Fannelop, T. K. and Flugge-Lotz, I., "Two-Dimensional Viscous Hypersonic Flow over Simple Blunt Bodies Including Second Order Effects," Rept. 144, May 1964, Stanford Univ., Palo Alto, Calif.